understand these mechanisms in detail, time-dependent SEC curves of the it-PMMA prepared by the st-PMAA host were obtained (Fig. 3). The curve with a single and narrow peak width shifted to a higher molecular weight, thereby supporting the latter mechanism, which is similar to living radical polymerization rather than conventional free-radical polymerization. We also suggest that the growing polymer chain migrates along the complementary template chain until the prepared nanospace is full. Although the curve was bimodal after 4 h, this is possibly due to the binding of terminal radicals in the film. As we stopped the polymerization of MMA after 3 h by opening the reaction vessel to the air, the radical terminals, which had been present in the films for at least 3 h, seemed to react with oxygen. The molecular weight of the st-PMMA prepared was similarly shifted, and a similar mechanism was supported.

This is, to our knowledge, the first report of an artificially constructed polymerization template and subsequent polymerization with the efficient transfer of structural information, similar to that seen in biosynthetic processes. Porous polymer matrices provided a reaction mould for stereoregular polymerization of methacrylates. It- and st-polymers with high stereoregularity and with a narrow molecular weight distribution were successfully prepared. Because particles coated with functional ultrathin films are readily handled and reusable (the porous films were reused at least 3 times), we expect large-scale synthesis of the stereoregular polymers to be achieved in the near future. Easier synthesis of stereoregular polymers of methacrylates potentiates their applications in technological and biomedical fields. Regulated nanospaces prepared in synthetic polymer assemblies should open the way to a new field of macromolecular recognition and synthesis. □

Methods

Assembly

The 9-MHz QCM with polished gold electrodes ($R_a = 1.8$ nm) was alternately immersed into the DMF solution of it-PMMA (1.7 mg ml^{-1}) and the DMF/water (2/3, v/v) solution of st-PMAA (1.5 mg ml^{-1}) for 5 min at 25 °C. After each immersion step, the QCM was gently rinsed with the same solvent, dried with nitrogen gas, and the frequency shift then measured. The shift was converted to the assembly amount by applying Sauerbrey's equation[8–11]. The assembly was initiated with it-PMMA in all cases.

Characterization

The QCM electrode with a refractive surface was used directly to observe the ATR spectra. The interferograms were co-added 50 times, and Fourier transformed at a resolution of 4 cm^{-1}. The film thickness was analysed by the scratching mode of an atomic force microscope (AFM). The roughness was also analysed by AFM. 400-MHz NMR (chloroform solvent) was used to analyse stereoregularity, in which *m* and *r* indicate the it and st-diads of meso and racemo, respectively. The triad (*mm*, *mr* and *rr*) and the tetrad (for example, *mmmm*) are represented similarly. SEC (THF solvent) was performed by PMMA standard.

Received 4 October 2003; accepted 29 March 2004; doi:10.1038/nature02525.

1. Alberts, B. *et al. Essential Cell Biology* 2nd edn (Garland, New York, 2003).
2. Buter, R., Tan, Y. Y. & Challa, G. Radical polymerization of methyl methacrylate in the presence of isotactic poly(methyl methacrylate). *J. Polym. Sci. A* **10,** 1031–1049 (1972).
3. Buter, R., Tan, Y. Y. & Challa, G. Radical polymerization of methyl methacrylate in the presence of stereoregular poly(methyl methacrylate). II. Syndiotactic PMMA as matrix. *J. Polym. Sci. Polym. Chem. Edn* **11,** 1003–1011 (1973).
4. Spěváček, J. & Schneider, R. Aggregation of stereoregular poly(methyl methacrylates). *Adv. Colloid Interface Sci.* **27,** 81–150 (1987).
5. Schomaker, E. & Challa, G. Complexation of stereoregular poly(methyl methacrylates). 14. The basic structure of the stereocomplex of isotactic and syndiotactic poly(methyl methacrylate). *Macromolecules* **22,** 3337–3341 (1989).
6. Buter, R., Tan, Y. Y. & Challa, G. Radical polymerization of methyl methacrylate in the presence of stereoregular poly(methyl methacrylate). III. Influence of temperature. *J. Polym. Sci. Polym. Chem.* **11,** 1013–1024 (1973).
7. Decher, G. in *Multilayer Thin Films* (eds Decher, G. & Schlenoff, J. B.) 1–46 (Wiley-VCH, Weinheim, 2003).
8. Serizawa, T. *et al.* Stepwise stereocomplex assembly of stereoregular poly(methyl methacrylate)s on a substrate. *J. Am. Chem. Soc.* **122,** 1891–1899 (2000).
9. Serizawa, T. *et al.* Stepwise assembly of isotactic poly(methyl methacrylate) and syndiotactic poly(methacrylic acid) on a substrate. *Langmuir* **16,** 7112–7115 (2000).
10. Hamada, K.-I. *et al.* Stepwise stereocomplex assembly of isotactic poly(methyl methacrylate) and syndiotactic poly(alkyl methacrylate)s on surfaces. *Langmuir* **17,** 5513–5519 (2001).
11. Serizawa, T., Hamada, K.-I., Kitayama, T. & Akashi, M. Recognition of stereoregular polymers using structurally-regulated ultrathin polymer films. *Angew. Chem. Int. Edn Engl.* **42,** 1118–1121 (2003).
12. Lohmeyer, J. H. G. M., Kransen, G., Tan, Y. Y. & Challa, G. Stereoassociation between poly(methyl methacrylate) and poly(methacrylic acid). *Polym. Lett. Edn* **13,** 725–729 (1975).
13. Lohmeyer, J. H. G. M., Tan, Y. Y., Lako, P. & Challa, G. Stereoselective association between isotactic poly(methyl methacrylate) and syndiotactic poly(methacrylic acid). *Polymer* **19,** 1171–1175 (1978).
14. Caruso, F., Caruso, R. A. & Möhwald, H. Nanoengineering of inorganic and hybrid hollow spheres by colloidal templating. *Science* **282,** 1111–1114 (1998).
15. Lohmeyer, J. H. G. M., Tan, Y. Y. & Challa, G. Polymerization of methacrylic acid in the presence of isotactic poly(methyl methacrylate) as possible template. *J. Macromol. Sci. A* **14,** 945–957 (1980).

Acknowledgements We thank K. Hatada and T. Kitayama for technological support of living anionic polymerization.

Competing interests statement The authors declare that they have no competing financial interests.

Correspondence and requests for materials should be addressed to M.A. (akashi@chem.eng.osaka-u.ac.jp).

Contribution of stratospheric cooling to satellite-inferred tropospheric temperature trends

Qiang Fu[1], Celeste M. Johanson[1], Stephen G. Warren[1] & Dian J. Seidel[2]

[1]*Department of Atmospheric Sciences, University of Washington, Seattle, Washington 98195, USA*
[2]*NOAA Air Resources Laboratory, Silver Spring, Maryland 20910, USA*

From 1979 to 2001, temperatures observed globally by the mid-tropospheric channel of the satellite-borne Microwave Sounding Unit (MSU channel 2), as well as the inferred temperatures in the lower troposphere, show only small warming trends of less than 0.1 K per decade (refs 1–3). Surface temperatures based on *in situ* observations however, exhibit a larger warming of ~0.17 K per decade (refs 4, 5), and global climate models forced by combined anthropogenic and natural factors project an increase in tropospheric temperatures that is somewhat larger than the surface temperature increase[6–8]. Here we show that trends in MSU channel 2 temperatures are weak because the instrument partly records stratospheric temperatures whose large cooling trend[9] offsets the contributions of tropospheric warming. We quantify the stratospheric contribution to MSU channel 2 temperatures using MSU channel 4, which records only stratospheric temperatures. The resulting trend of reconstructed tropospheric temperatures from satellite data is physically consistent with the observed surface temperature trend. For the tropics, the tropospheric warming is ~1.6 times the surface warming, as expected for a moist adiabatic lapse rate.

The inconsistency between the trends at the surface and in the troposphere, traceable to the pioneering work of ref. 10, has raised questions about the ability of current global climate models (GCMs) to predict climate changes, the reliability of the observational data used to derive temperature trends, and the reality of human-induced climate change[4,11–15]. It is generally agreed that the warming trend in global-mean surface temperature observations during the past 20 years is real and at least partly of anthropogenic origin[4,12]. This increase of temperature is supported by observations of a reduction of snow cover and sea ice, thawing of permafrost, changes in freeze/thaw dates of lake and river ice, ocean warming and sea-level rise, and other related environmental changes[4]. However, the situation is less clear for tropospheric temperatures. Balloon-borne radiosondes have been the principal tool for atmospheric profiling. From 1979 to 2001, the trends of tropospheric-layer temperature between 850 and 300 hPa, as derived from different radiosonde data sets[3], range from −0.03 to +0.04 K per decade. The radiosondes have limited spatial coverage, particularly

over large parts of the oceans, and are subject to a host of complications, including changing instrument types and observation practices[16,17], which confound analyses of climate trends.

The MSU, since 1979, and its successor, the Advanced MSU (AMSU), from 1998, provide a global measure of temperature for several atmospheric layers from NOAA polar-orbiting satellites. Although the original purpose of MSU measurements was to improve weather forecasts, a continuing data-analysis effort has been made to satisfy climate research requirements of homogeneity and calibration[1,2,10,18–24]. Several important non-climatic influences have been identified and removed, including diurnal temperature biases related to local sampling times of the satellite and their changes over its lifetime, errors in the MSU calibration, and biases due to decay of the satellite orbits. Recent analyses of MSU channel 2 (most sensitive to the mid-troposphere) by the University of Alabama at Huntsville (UAH) and the Remote Sensing Systems (RSS) teams find temperature trends of 0.01 K per decade[1] and 0.1 K per decade[2], respectively, during 1979–2001. This trend difference is mainly due to differences in data adjustments related to instrument calibration and diurnal drift correction[2]. The purpose of this Letter is not to reconcile the trend differences between these two research teams, but to address the question of whether the MSU data really imply small or negligible tropospheric warming over the past two decades. We argue that the trends reported by both teams for the 'mid-tropospheric' channel are substantially smaller than the actual trend of the mid-tropospheric temperature.

To infer the temperature of the mid-troposphere, we use two microwave channels: MSU channels 2 and 4 (or AMSU channels 5 and 9). Their weighting functions are shown in Fig. 1a. The weighting function for MSU channel 2 (or AMSU channel 5) peaks at ~550 hPa (~4.5 km). Thus the MSU Channel 2 brightness temperatures (T_2) have often been used to represent mid-tropospheric temperatures[1,2,3,8,15,22,24]. The MSU channel 4 (or AMSU channel 9), whose weighting function peaks at ~85 hPa (~18 km), has been used to represent stratospheric temperatures[1,3,8,15].

As ~85% of the signal for T_2 comes from the troposphere and surface, it is not a bad approximation to say that the seasonal and interannual variations of mean deep-layer temperature in the troposphere can be well represented by T_2. However, this might not be the case for trends. Figure lb shows simulated changes of T_2 owing to changes of tropospheric and stratospheric temperatures, and indicates that T_2 remains constant when the changes in tropospheric and stratospheric temperatures have a ratio of about −1/5. This is because the vertical integral of the weighting function from the surface to tropopause, near 200 hPa, is about 5 times the integral above the tropopause. For example, if the tropospheric temperature trend were 0.15 K per decade and the stratospheric trend were −0.8 K per decade, the trend of T_2 would be close to zero. Intriguingly, this scenario resembles what may actually be the case in the atmosphere. The temperature trend in the lower stratosphere (15 to 23 km), as obtained from radiosondes and satellite observations, is about −0.5 to −0.9 K per decade for the last 20 years[1,3,4,9]. Therefore, because of the combined influence of stratospheric and tropospheric changes, T_2 trends are not an ideal indicator of global climate change. To derive the tropospheric temperature trends, the effects of stratospheric cooling on T_2 must be taken into account.

Although a stratospheric influence on the T_2 trend has long been recognized[20,25,26], it has never been well quantified. The UAH team created a synthetic channel called T_{2LT}, where LT means 'low-middle troposphere'[1,19,25], by subtracting signals at different view-angles of MSU channel 2. However, this approach amplifies noises, increases satellite inter-calibration biases, and may introduce other complications involving effects of changes in surface emissivity and of mountainous terrain[2,19,20,24–28]. For these reasons, the T_{2LT} record is now receiving less attention than the better-calibrated T_2 record[2,15,22,24]. Here we develop an alternative method to remove the stratospheric contribution, which should be free of the complications afflicting T_{2LT}, by making use of data from MSU channel 4.

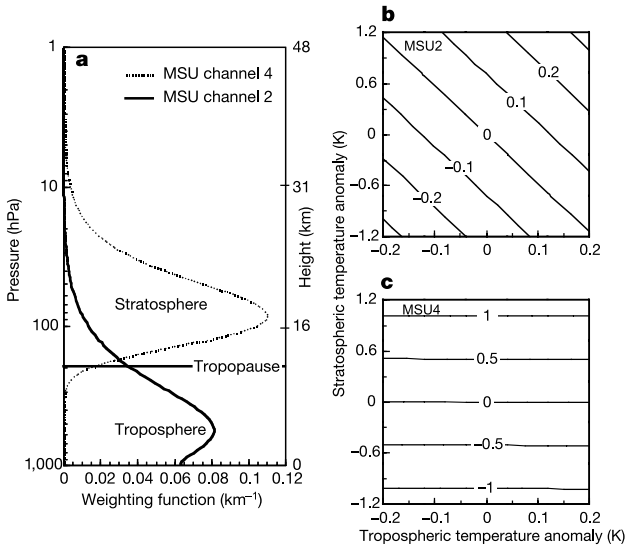

Figure 1 Atmospheric weighting functions and brightness temperature responses. **a**, Weighting function profiles for MSU channels 2 and 4 over ocean[1,2]. The boundary between the troposphere and the stratosphere (the tropopause) is shown at 200 hPa. The satellite-observed brightness temperature, T_b, can be expressed in the form:

$$T_b = T_s W_s + \int_0^\infty T(z)W(z)dz$$

where T_s is the surface temperature, W_s the surface contribution factor, $T(z)$ the atmospheric temperature profile, and $W(z)$ the weighting function. Thus the weighting function describes the relative contributions of atmospheric temperatures at different heights to the brightness temperatures observed by the satellite. **b**, Responses of MSU channel 2 brightness temperature to changes in stratospheric and tropospheric temperatures assuming a US Standard Atmosphere and a surface emissivity of 0.5. Contours and axes are both labelled in K. **c**, Same as **b** but for MSU channel 4.

The MSU channel 4 brightness temperature (T_4) is sensitive mainly to stratospheric temperature changes (Fig. lc), so it can be used to remove the contribution of the stratosphere to T_2. We define the free-tropospheric temperature as the mean temperature between 850 and 300 hPa ($T_{850\text{-}300}$; ref. 3). We derive this temperature from the measured brightness temperatures of MSU channels 2 and 4, as:

$$T_{850-300} = a_0 + a_2 T_2 + a_4 T_4 \quad (1)$$

To obtain these three coefficients, we use global-, hemispheric- and tropical-average monthly temperature anomaly profiles from radiosonde observations at 87 stations, for the period 1958–97 (ref. 17). The radiosonde data at the surface and at 15 pressure levels between 1,000 and 10 hPa are used to derive temperature anomalies for the 850–300-hPa layer as well as for MSU channels 2 and 4 (ref. 3). The coefficients in equation (1) are then obtained by least-squares regression (see Supplementary Table 1 for the values). For global-average anomalies, a_2 is 1.156 and a_4 is −0.153. The effective vertical weighting function for $T_{850\text{-}300}$ (that is, $a_2W_2 + a_4W_4$, where $W_{2,4}$ are the physical weighting functions for $T_{2,4}$) peaks at the same level as T_2 but is 15% larger. In the stratosphere it is negative above ~100 hPa and positive below, so that the integrated contribution of the stratosphere becomes near-zero. The effective weighting function may have a negative part[25]; this is different from the physical weighting function, which must be positive everywhere.

The success of equation (1) in predicting $T_{850\text{-}300}$ from T_2 and T_4 is shown in Supplementary Fig. 1. The global-average anomalies of 850–300-hPa layer temperature, as derived from the radiosonde-simulated T_2 and T_4, closely follow those directly observed by radiosondes for the period 1958–79. The correlation coefficient is 0.984, with a root-mean-square error of 0.065 K. The trend differences are only about 0.001 K per decade. The T_4 time series can

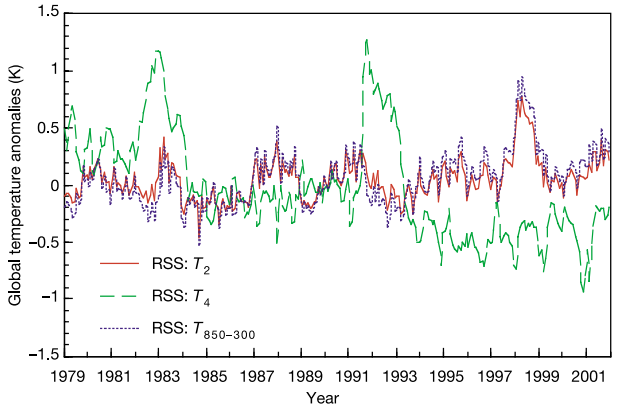

Figure 2 Time series of monthly mean, global-average temperature anomalies. Shown are the MSU channel 2 brightness temperature (T_2), MSU channel 4 brightness temperature (T_4) and MSU-derived 850–300-hPa layer temperature ($T_{850\text{-}300}$), based on the MSU data as analysed by the RSS team. All data are expressed as anomalies relative to climatological monthly means over 1985–94.

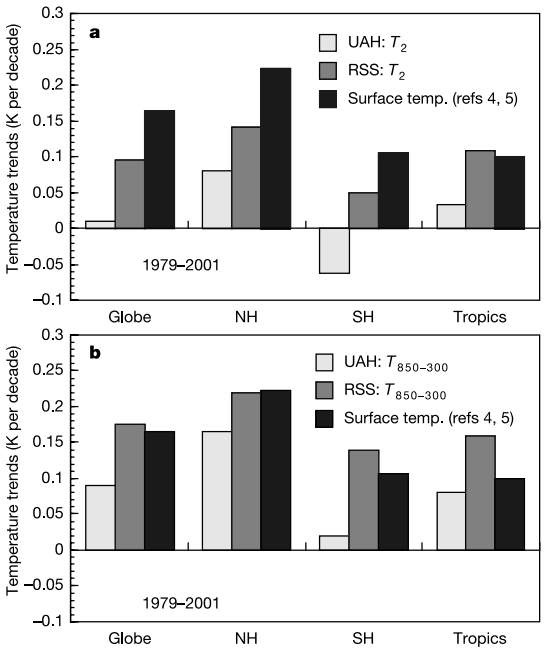

Figure 3 Trends in monthly mean temperature anomalies. **a**, MSU channel 2 brightness temperature trend and **b**, MSU-derived 850–300-hPa layer temperature trend for the globe, Northern Hemisphere (NH), Southern Hemisphere (SH) and tropics (30° N–30° S). The results using both UAH (version 5) and RSS data sets are shown. See Supplementary Table 2 for these trend values and their error estimates. The surface temperature trends are also shown for comparison. The surface temperature trends for the globe, Northern Hemisphere and Southern Hemisphere are from ref. 5; the surface trend for the tropical region is from ref. 4.

therefore be used to remove nearly all of the contribution of the stratosphere to T_2 in the trend analyses. This is because temperature variations in the stratosphere are vertically coherent and well correlated with T_4.

We now apply equation (1) to satellite-observed time series of T_2 and T_4 from 1979 to 2001, as reported by UAH[1] and RSS[2], to derive $T_{850\text{-}300}$. The global anomaly time series of $T_{850\text{-}300}$ using RSS data is shown in Fig. 2, along with those of T_2 and T_4. It is evident that the $T_{850\text{-}300}$ trend is more positive than the T_2 trend. (Similar results are obtained using UAH data, not shown here.)

Figure 3 shows the trends for T_2 (Fig. 3a) and MSU-derived $T_{850\text{-}300}$ (Fig. 3b) for the globe, Northern Hemisphere, Southern Hemisphere, and tropics (30° N–30° S) using both the UAH and RSS datasets, as well as surface temperature trends based on *in situ* observations[4,5]. The trends of 0.01 K per decade (UAH) and 0.1 K per decade (RSS) for global mean T_2 are substantially smaller than the surface temperature trend of 0.17 K per decade. In the Southern Hemisphere, the T_2 trend from UAH is actually negative. However, as shown in Fig. 3b, the global trends of $T_{850\text{-}300}$ are 0.09 K per decade (UAH) and 0.18 K per decade (RSS), which are about 0.08 K per decade larger than the corresponding T_2 trends. The trend difference between $T_{850\text{-}300}$ and T_2 for the tropics is smaller (~0.05 K per decade) because there the tropopause is higher and the stratospheric cooling is smaller, so the stratospheric influence is smaller.

Our analysis of the RSS data set suggests that over the past 22 years the global free troposphere has warmed at close to the same rate as the surface. The ratio of free-tropospheric temperature trend to surface temperature trend is ~1.1 for the globe and 1.6 for the tropics. In the tropics where the temperature follows the moist adiabatic lapse rate[29], this ratio should be larger than unity[14,28,30]. GCM studies have predicted a global ratio of ~1.2 (ref. 8) and a tropical ratio of ~1.54 (ref. 14). Note that the RSS T_2 trend is also statistically consistent with a GCM prediction of T_2 (ref. 15).

Applying the stratospheric corrections to the UAH data set also enhances the mid-tropospheric temperature trends, but they are still smaller than the surface warming rate, particularly over the Southern Hemisphere (Fig. 3b). In addition, the UAH-reported T_{2LT} (bulk temperatures for the low–middle troposphere) seems to be inconsistent with the $T_{850\text{-}300}$ obtained from the UAH data. For example, over the period from 1979 to 2001, the UAH-reported T_{2LT} trend in the tropics is −0.01 K per decade, which is substantially smaller than the $T_{850\text{-}300}$ trend of 0.08 K per decade. (The trend of the difference time series between $T_{850\text{-}300}$ and T_{2LT} (that is, $T_{850\text{-}300} - T_{2LT}$), which is 0.09 ± 0.05 K per decade (the 95% confidence interval), is significantly different from zero at less than 0.1% significance level.) Also note that in the tropics the UAH T_{2LT} is cooling at −0.04 k per decade relative to the UAH T_2. This apparent inconsistency may be attributed to complications involving the T_{2LT} retrieval, as well as to the techniques used by UAH to analyse the MSU channel 2 data, which could also explain the lack of agreement between GCM simulations[8] and UAH results for the trend differences of either $T_s - T_{2LT}$, where T_s is the surface temperature, or $T_s - T_2$, despite their agreement for T_2 trends[8].

In an independent analysis of MSU data, Vinnikov and Grody[24] found a large positive global trend of 0.22–0.26 K per decade for T_2, which they used to represent the tropospheric temperature. But irrespective of the techniques used to analyse the data, T_2 is subject to the effects of stratospheric cooling. Assuming a stratospheric temperature trend of −0.5 K per decade[1,3,4], the Vinnikov–Grody T_2 trend translates to a $T_{850\text{-}300}$ trend of ~0.33–0.37 K per decade. This value is about twice as large as the surface warming globally. It also suggests a ratio of ~3 between tropospheric and surface temperature trends for the tropical region. These ratios seem large, and suggest that the technique Vinnikov and Grody used to analyse the satellite data may require further scrutiny. □

Received 8 December 2003; accepted 29 March 2004; doi:10.1038/nature02524.

1. Christy, J. R. *et al.* Error estimates of version 5.0 of MSU-AMSU bulk atmospheric temperatures. *J. Atmos. Ocean. Technol.* **20,** 613–629 (2003).
2. Mears, C. A., Schabel, M. C. & Wentz, F. J. A reanalysis of the MSU channel 2 tropospheric temperature record. *J. Clim.* **16,** 3650–3664 (2003).
3. Seidel, D. J. *et al.* Uncertainty in signals of large-scale climate variations in radiosonde and satellite upper-air temperature datasets. *J. Clim.* (in the press).
4. Houghton, J. T. *et al.* in *Climate Change 2001: The Scientific Basis* (Cambridge Univ. Press, London, 2001).
5. Jones, P. D. & Moberg, A. Hemispheric and large-scale surface air temperature variations: An extensive revision and an update to 2001. *J. Clim.* **16,** 206–223 (2003).
6. Bengtsson, L., Roeckner, E. & Stendel, M. Why is the global warming proceeding much slower than expected? *J. Geophys. Res.* **104,** 3865–3876 (1999).

7. Santer, B. D. *et al.* Interpreting differential temperature trends at the surface and in the lower troposphere. *Science* **287,** 1227–1232 (2000).
8. Hansen, J. *et al.* Climate forcings in Goddard Institute for Space Studies SI2000 simulations. *J. Geophys. Res.* **107,** doi:10.1029/2001JD001143 (2002).
9. Ramaswamy, V. *et al.* Stratospheric temperature trends: Observations and model simulations. *Rev. Geophys.* **39,** 71–122 (2001).
10. Spencer, R. W. & Christy, J. R. Precise monitoring of global temperature trends from satellites. *Science* **247,** 1558–1662 (1990).
11. Hansen, J. *et al.* Satellite and surface temperature data at odds? *Clim. Change* **30,** 103–117 (1995).
12. Wallace, J. M. *et al. Reconciling Observations of Global Temperature Change* (National Academy Press, Washington DC, 2000).
13. Singer, S. F. Difficulty in reconciling global warming data. *Nature* **409,** 281 (2001).
14. Hegerl, G. C. & Wallace, J. M. Influence of patterns of climate variability on the difference between satellite and surface temperature trends. *J. Clim.* **15,** 2412–2428 (2002).
15. Santer, B. D. *et al.* Influence of satellite data uncertainties on the detection of externally forced climate change. *Science* **300,** 1280–1284 (2003).
16. Gaffen, D. J., Sargent, M. A., Habermann, R. E. & Lanzante, J. R. Sensitivity of tropospheric and stratospheric temperature trends to radiosonde data quality. *J. Clim.* **13,** 1776–1796 (2000).
17. Lanzante, J. R., Klein, S. A. & Seidel, D. J. Temporal homogenization of monthly radiosonde temperature data. *J. Clim.* **16,** 224–262 (2003).
18. Christy, J. R., Spencer, R. W. & McNider, R. T. Reducing noise in the MSU daily lower-tropospheric global temperature dataset. *J. Clim.* **8,** 888–896 (1995).
19. Christy, J. R., Spencer, R. W. & Lobl, E. S. Analysis of the merging procedure for the MSU daily temperature time series. *J. Clim.* **11,** 2016–2041 (1998).
20. Wentz, F. J. & Schabel, M. Effects of orbital decay on satellite-derived lower-tropospheric temperature trends. *Nature* **394,** 661–664 (1998).
21. Christy, J. R., Spencer, R. W. & Braswell, W. D. MSU tropospheric temperature: Dataset construction and radiosonde comparisons. *J. Atmos. Ocean. Technol.* **17,** 1153–1170 (2000).
22. Prabhakara, C., Iacovazzi, J. R., Yoo, J. M. & Dalu, G. Global warming: Evidence from satellite observations. *Geophys. Res. Lett.* **27,** 3517–3520 (2000).
23. Mo, T., Goldberg, M. D. & Crosby, D. S. Recalibration of the NOAA microwave sounding unit. *J. Geophys. Res.* **106,** 10145–10150 (2001).
24. Vinnikov, K. Y. & Grody, N. C. Global warming trend of mean tropospheric temperature observed by satellites. *Science* **302,** 269–272 (2003).
25. Spencer, R. W. & Christy, J. R. Precision and radiosonde validation of satellite gridpoint temperature anomalies. Part II: A tropospheric retrieval and trends during 1979–1990. *J. Clim.* **5,** 858–866 (1992).
26. Hurrell, J. W. & Trenberth, K. E. Spurious trends in satellite MSU temperature from merging different satellite records. *Nature* **386,** 164–167 (1997).
27. Trenberth, K. E. & Hurrell, J. W. Reply to "How accurate are satellite 'thermometers'?". *Nature* **389,** 342–343 (1997).
28. Hurrell, J. W. & Trenberth, K. E. Difficulties in obtaining reliable temperature trends: Reconciling the surface and satellite Microwave Sounding Unit records. *J. Clim.* **11,** 945–967 (1998).
29. Stone, P. H. & Carlson, J. H. Thermal equilibrium of the atmosphere with a given distribution of relative humidity. *J. Atmos. Sci.* **36,** 415–423 (1979).
30. Wentz, F. J. & Schabel, M. Precise climate monitoring using complementary satellite data sets. *Nature* **403,** 414–416 (2000).

Supplementary Information accompanies the paper on **www.nature.com/nature**.

Acknowledgements We thank J. M. Wallace for discussions. We also thank J. M. Wallace, D. L. Hartmann, J. R. Holton, J. K. Angell and M. Free for their comments on the manuscript. This study was supported by the US DOE, NSF and NASA.

Competing interests statement The authors declare that they have no competing financial interests.

Correspondence and requests for materials should be addressed to Q.F. (qfu@atmos.washington.edu).

Partitioning of oxygen during core formation on the Earth and Mars

David C. Rubie, Christine K. Gessmann* & Daniel J. Frost

Bayerisches Geoinstitut, University of Bayreuth, D-95444 Bayreuth, Germany

* Present address: Gleiwitzerstrasse 3, D-55131 Mainz, Germany

Core formation on the Earth and Mars involved the physical separation of metal and silicate, most probably in deep magma oceans[1–4]. Although core-formation models explain many aspects of mantle geochemistry, they have not accounted for the large differences observed between the compositions of the mantles of the Earth (~8 wt% FeO) and Mars (~18 wt% FeO) or the smaller mass fraction of the martian core[5–7]. Here we explain these differences as a consequence of the solubility of oxygen in liquid iron-alloy increasing with increasing temperature. We assume that the Earth and Mars both accreted from oxidized chondritic material. In a terrestrial magma ocean, 1,200–2,000 km deep, high temperatures resulted in the extraction of FeO from the silicate magma ocean owing to high solubility of oxygen in the metal. Lower temperatures of a martian magma ocean resulted in little or no extraction of FeO from the mantle, which thus remains FeO-rich. The FeO extracted from the Earth's magma ocean may have contributed to chemical heterogeneities in the lowermost mantle[8], a FeO-rich D″ layer[9] and the light element budget of the core[10,11].

The most significant differentiation event in the history of the Earth and other terrestrial planets was the separation of metal and silicate to form a metallic Fe-rich core and a silicate mantle. The geochemical consequences of this process have been studied extensively in recent years to explain the geochemistry of the Earth's mantle and the physical mechanisms of core formation and accretion. Extensive melting of the Earth and the formation of a deep magma ocean as a consequence of one or more giant impacts probably facilitated metal–silicate separation[12,13]. The content of moderately siderophile (metal-loving) elements, such as Ni and Co, in the Earth's mantle can be explained by the separation of liquid metal and silicate in a magma ocean at least 700 km deep[1–3]. This conclusion is based on experimental studies of the partitioning of siderophile elements between liquid metal and liquid silicate at high pressure. Here we consider the partitioning of oxygen between metal and silicate in a magma ocean with the aim of understanding how the FeO content and oxidation state of planetary mantles are affected by core formation.

We studied the solubility of oxygen in liquid Fe-Ni alloy at 9 and 18 GPa, 2,173–2,673 K and oxygen fugacities (f_{O_2}) 1.1 to 3.6 log units below the iron-wüstite buffer by equilibrating the samples with magnesiowüstite in a multianvil apparatus. Details of the starting materials and experimental and analytical methods have been described previously[14]. Over the range of experimental conditions, the solubility varies from below detection limit to 1.28 wt% (Fig. 1a, Table 1). The results show that oxygen solubility increases with increasing temperature and oxygen fugacity (Fig. 1a). To determine the effects of pressure and temperature independently of f_{O_2}, we calculate the distribution coefficient, K_d, for the partitioning of oxygen between liquid Fe-alloy and magnesiowüstite:

$$K_d = \frac{X_O^{met} X_{Fe}^{met}}{X_{FeO}^{mw}} \quad (1)$$

where X_O^{met}, X_{Fe}^{met} and X_{FeO}^{mw} are the mole fractions of oxygen in metal, Fe in metal and FeO in magnesiowüstite respectively. As shown in Fig. 1b, the distribution coefficient, and therefore the oxygen solubility at constant f_{O_2}, decreases with increasing pressure. These trends are consistent with previous results obtained at 5–25 GPa and 2,073–2,773 K but over a relatively restricted f_{O_2} range[15]. Note that the results are contrary to early predictions that the solubility of oxygen in liquid Fe should increase with increasing pressure[16].

To extrapolate the oxygen solubility data as a function of pressure (P) and temperature (T), we use:

$$RT\ln K_d = -\Delta H + T\Delta S - P\Delta V \quad (2)$$

where ΔH, ΔS and ΔV are the changes in enthalpy, entropy and volume, respectively, for the oxygen exchange reaction and R is the gas constant. We fitted equation (2) to the data, including five experimental results obtained up to 25 GPa by ref. 15. Results of the fit, shown in Fig. 1a and b, give $\Delta H = 153{,}000\ (\pm 29{,}000)$ J mol^{-1}, $\Delta S = 50.9\ (\pm 12.4)$ J K^{-1} mol^{-1} and $\Delta V = 1{,}448\ (\pm 440)$ J GPa^{-1} (1.448 ± 0.44 cm^3 mol^{-1}).

Extrapolations of the solubility results to higher pressures and